THE JOURNAL OF PHYSICAL CHEMISTRY C

ARTICLE

pubs.acs.org/JPCC

Screening Metal−Organic Frameworks by Analysis of Transient Breakthrough of Gas Mixtures in a Fixed Bed Adsorber

Rajamani Krishna*,† and Jeffrey R. Long‡

†Van't Hoff Institute for Molecular Sciences, University of Amsterdam, Science Park 904, 1098 XH Amsterdam, The Netherlands

‡Department of Chemistry, University of California, Berkeley, Berkeley, California 94704, United States, and Materials Sciences Division, Lawrence Berkeley National Laboratory, Berkeley, California 94720-1460, United States

Supporting Information

ABSTRACT: Metal−organic frameworks (MOFs) offer considerable potential for separating a variety of mixtures that are important in applications such as CO_2 capture and H_2 purification. In view of the vast number of MOFs that have been synthesized, there is a need for a reliable procedure for comparing screening and ranking MOFs with regard to their anticipated performance in pressure swing adsorption (PSA) units. For this purpose, the most commonly used metrics are the adsorption selectivity and the working capacity. Here, we suggest an additional metric for comparing MOFs that is based on the analysis of the transient response of an adsorber to a step input of a gaseous mixture. For a chosen purity of the gaseous mixture exiting from the adsorber, a dimensionless breakthrough time τ_{break} can be defined and determined; this metric determines the frequency of required regeneration and influences the productivity of a PSA unit. The values of τ_{break} are dictated both by selectivity and by capacity metrics .By performing transient adsorber calculations for separation of CO_2/H_2, CO_2/CH_4, CH_4/H_2, and $CO_2/CH_4/H_2$ mixtures, we compare the values of τ_{break} to highlight some important advantages of MOFs over conventionally used adsorbents such as zeolite NaX. For a given separation duty, such comparisons provide a more realistic ranking of MOFs than afforded by either selectivity or capacity metrics alone. We conclude that breakthrough calculations can provide an essential tool for screening MOFs.

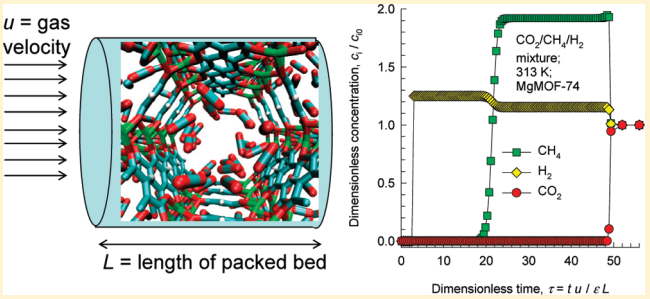

1. INTRODUCTION

Metal−organic frameworks (MOFs) constitute a broad new class of materials in which metal ions or clusters are connected via lightweight organic bridging ligands to form a porous three-dimensional network structure. Owing to their high specific surface areas and tunable pore sizes, these materials have come under intense investigation for possible applications in gas storage.[1−3] More recently, the development of synthetic methods for adjusting the chemical functionality on the surfaces within MOF structures has led to interest in utilizing them for the separation of various gas mixtures.[4] Here, MOFs can provide some key advantages as selective adsorbents: large pore sizes enabling rapid diffusion kinetics, tunable binding strengths affecting selectivity, and high surface areas that can result in a large working capacity.

A substantial amount of the published research on metal−organic frameworks (MOFs) is dedicated to the issue of CO_2 capture by selective adsorption.[4−9] With MOFs, a wide variety of strategies can be adopted to enhance the CO_2 uptake; these include appropriate choice of ligand design,[10] the introduction of nonframework cations,[11,12] use of exposed metal cation sites,[13−16] and post-synthetic modification by introduction of polar surface groups.[17] The adsorption selectivities are also enhanced by incorporation of special functional groups within a framework.[18−26] For example, Couck et al.[24] demonstrated that functionalizing the MIL-53(Al) framework with amino groups increases its selectivity in CO_2/CH_4 separations by orders of magnitude while maintaining a very high capacity for CO_2 capture.

It is customary to compare or screen MOFs on the basis of the adsorption *selectivity*, S_{ads}, defined for separation of a binary mixture of species 1 and 2 by

$$S_{ads} = \frac{q_1/q_2}{p_1/p_2} \qquad (1)$$

where the q_i represent the molar loadings within the porous material that is in equilibrium with a bulk gas phase with partial pressures p_i. The S_{ads} values can be estimated using experimental data on the pure components isotherms, along with the Ideal Adsorbed Solution Theory (IAST) of Myers and Prausnitz for binary adsorption equilibrium.[27] As illustration, Figure 1a presents IAST estimates of S_{ads} for separation of a 20/80 CO_2/H_2 mixture relevant to H_2 purification using NaX and five different MOFs: [7] MgMOF-74,[13,14,16,28−30] MOF-177,[31] CuBTTri,[23]

Received: March 8, 2011
Revised: May 29, 2011
Published: June 02, 2011

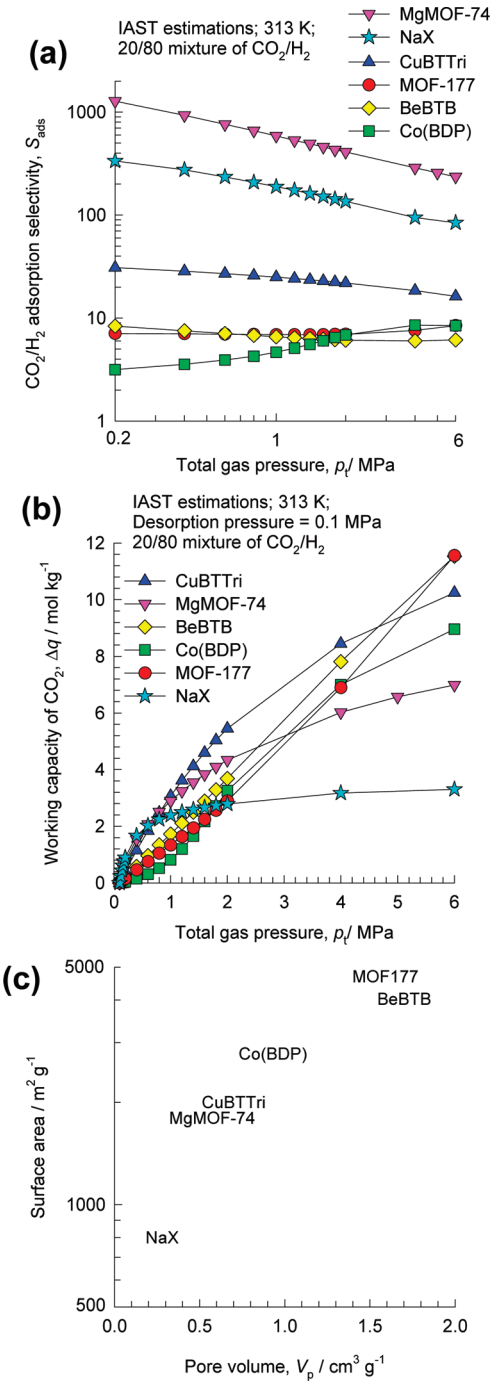

Figure 1. Calculations using IAST of (a) adsorption selectivity, S_{ads}, and (b) working capacity of CO_2, Δq, for separation of 20/80 CO_2/H_2 mixture at 313 K using MgMOF-74, MOF-177, Co(BDP), CuBTTri, BeBTB, and zeolite NaX. For calculation of Δq, the desorption pressure is chosen as 0.1 MPa. The composition of the gas mixture at the desorption pressure is maintained at 20/80 CO_2/H_2.The dual-site Langmuir−Freundlich fits of the pure component isotherms for CO_2 and H_2 adsorption isotherms are based on the experimental data of Herm et al.[37] and Belmabkhout et al.[76] The Supporting Information accompanying this publication contains the dual Langmuir−Freundlich fit constants. Also contained here are validations of the IAST calculations using Configurational-Bias Monte Carlo simulations of mixture adsorption. (c) Data on surface area and pore volumes for selected MOFs and NaX, taken from Herm et al.[37]

BeBTB,[32] and Co(BDP).[33,34] By this means of comparison, MgMOF-74 (also denoted as CPO-27-Mg, or Mg_2(dobdc) with dobdc = ($dobdc^{4-}$ = 1,4-dioxido-2,5-benzenedicarboxylate) emerges as the adsorbent with the highest S_{ads} over the entire range of pressures.

Besides S_{ads}, another important factor that determines the economics of PSA units is the working capacity, or "delta loading", Δq.[35−37] This metric is defined as the difference in the loadings of the component that needs to be preferentially adsorbed, expressed in moles per kilogram of microporous crystalline material, at the "adsorption" pressure minus the corresponding loading at the "desorption", or purge, pressure. The adsorption pressure could be in the 0.1−10 MPa range, and the desorption pressure could be 0.01−0.1 MPa. Figure 1b shows IAST estimates of the working capacity of CO_2 for adsorption from a 20/80 CO_2/H_2 mixture. Note that all five MOFs have larger working capacities than NaX for operation at total pressures p_t > 2 MPa. As pore saturation conditions are approached at high pressures, the hierarchy of Δq is dictated largely by the pore volumes and surface areas; cf. Figure 1c.

For a PSA unit operating at say 6 MPa, screening on the basis of S_{ads} indicates MgMOF-74 as the best choice. If we use Δq for ranking, then BeBTB and MOF-177 emerge as better choices. This dilemma indicates the need to examine PSA operations in more detail. On the basis of a careful analysis of the variety of factors that affect PSA performance, Kumar[38] concluded that neither highest S_{ads} nor maximum Δq on its own can be chosen as the criterion for adsorbent selection; rather, it is the combination of S_{ads} and Δq which leads to the best adsorbent. Ho et al.[35] have demonstrated that both S_{ads} and Δq determine the cost of CO_2 capture in a PSA unit. The primary aim of the work presented here is to suggest a further metric that reflects the right combination of S_{ads} and Δq needed to establish a representative indicator of PSA performance. The approach we adopt requires us to analyze the transient breakthrough of gas mixtures at the outlet of an adsorber. For a specified purity of the exiting gas mixture, we aim to show that the corresponding breakthrough times reflect the right combination of S_{ads} and Δq. These breakthrough times are more easily relatable to productivity and costs of a PSA unit. In several experimental studies, breakthrough curves and breakthrough times are used to evaluate the separation performance of a specific adsorbent[13,39] or to screen a variety of adsorbents for a specified separation.[40,41] Rather than perform such experiments, which are labor-intensive and can present a range of technical challenges to achieve accurate results, we *calculate* the breakthrough characteristics using reliable pure component gas adsorption isotherm data as inputs.

In order to demonstrate the applicability of the suggested approach, we consider separation of CO_2/H_2, CO_2/CH_4, CH_4/H_2, and $CO_2/CH_4/H_2$ mixtures using a variety of MOFs. The specific MOFs employed were selected as representative of several prominent subclasses of these materials: rigid frameworks with high surface areas (MOF-177 and BeBTB), frameworks with surfaces bearing a high concentration of coordinatively unsaturated metal cation sites (MgMOF-74 and CuBTTri), and a flexible framework exhibiting large pressure-dependent changes in pore volume (Co(BDP)).

2. MODEL FOR TRANSIENT ADSORBER DYNAMICS

Consider a fixed bed adsorber, of length L, containing MOF crystals; cf. Figure 2. Assuming plug flow of an n-component gas

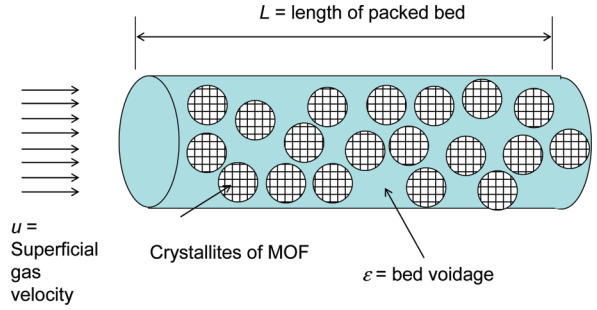

Figure 2. Schematic of a packed bed adsorber.

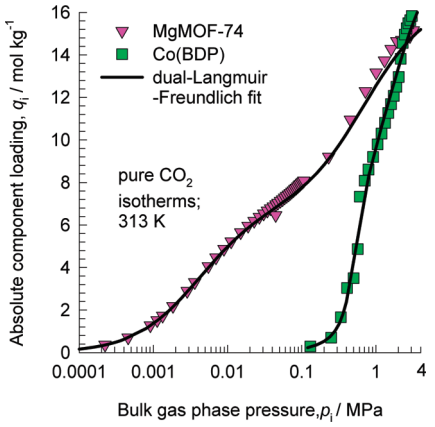

Figure 3. Dual-site Langmuir−Freundlich fits of the CO_2 adsorption isotherms for MgMOF-74 and Co(BDP) at 313 K. The fits are based on the experimental data of Herm et al.[37] The Supporting Information accompanying this publication contains the dual-Langmuir-Freundlich fit constants.

mixture through a fixed bed maintained under isothermal conditions and negligible pressure drop, the partial pressures in the gas phase at any position and instant of time are obtained by solving the following set of partial differential equations for each of the species i in the gas mixture.[42−48]

$$\frac{1}{RT}\frac{\partial p_i}{\partial t} = -\frac{1}{RT}\frac{\partial (up_i)}{\partial z} - (1-\varepsilon)\rho\frac{\partial \overline{q}_i}{\partial t} \qquad (2)$$

$$i = 1, 2, \ldots, n$$

In eq 2, t is the time, z is the distance along the adsorber, ρ is the MOF framework density, ε is the bed voidage, and $\overline{q}_i$ is the average loading within the MOF crystallites of radius r_c

$$\overline{q}_i = \frac{3}{r_c^3}\int_0^{r_c} q_i r^2\, dr \qquad (3)$$

The radial distribution of molar loadings, q_i, within each crystallite is obtained from a solution of a set of differential equations describing the uptake within a crystallite

$$\frac{\partial q_i}{\partial t} = -\frac{1}{\rho}\frac{1}{r^2}\frac{\partial}{\partial r}(r^2 N_i) \qquad (4)$$

The fluxes N_i, in turn, are related to the radial gradients in the loading, $\partial q_i/\partial r$, by the Maxwell−Stefan formulation of intracrystalline diffusion.[48−51]

The molar loadings q_i at the outer surface of the crystallites, i.e., at $r = r_c$, are calculated on the basis of adsorption equilibrium with the bulk gas phase partial pressures p_i at that position z and time t. In applying the IAST, it is necessary to have reliable fits of the pure component isotherm data over a wide range of pressures. The isotherm model should be capable of describing the inflection characteristics such as that observed for CO_2 adsorption in some MOFs.[30,37] As an illustration, Figure 3 shows the experimental CO_2 isotherms for MgMOF-74 and Co(BDP) at 313 K. The inflection in the MgMOF-74 data is very pronounced and occurs at a loading corresponding to one CO_2 molecule per Mg atom in the framework.[30] The inflection characteristics of Co(BDP) instead have their origin in guest-induced structural transformations.[33,34] The inflection behaviors of both of these MOFs are adequately captured by the dual-site Langmuir−Freundlich isotherm

$$q_i = q_{i,A,sat}\frac{b_{i,A}p_i^{\nu_{i,A}}}{1+b_{i,A}p_i^{\nu_{i,A}}} + q_{i,B,sat}\frac{b_{i,B}p_i^{\nu_{i,B}}}{1+b_{i,B}p_i^{\nu_{i,B}}} \qquad (5)$$

Use of eq 5 is also required for adsorption of CO_2 in MOFs at temperatures below its critical temperature, $T_c = 301$ K.[52] Owing to cluster formation, the isotherms become increasingly steeper as the temperature is lowered below T_c;[53,54] the steepness of these isotherms can be properly captured provided at least one of the exponents ν_i exceeds unity.

It is worth noting that in most of the published literature on PSA modeling,[43] the mixed-gas Langmuir model

$$q_i = q_{i,sat}\frac{b_i p_i}{1+\sum_{j=1}^{n} b_j p_j} \qquad (6)$$

is commonly used for calculation of mixture equilibrium, along with single-site Langmuir fits of the pure component isotherms. The use of mixed-gas Langmuir model yields

$$S_{ads} = \frac{q_{1,sat}b_1 p_2}{q_{2.sat}b_2 p_1} \qquad (7)$$

Equation 7 predicts S_{ads} to be *independent* of p_t. This approach is thermodynamically inconsistent, except when the saturation adsorption capacities of all component species are equal.[55] The inconsistency is particularly evident for CO_2/H_2 mixtures, because the saturation capacity of H_2 is significantly higher than that for CO_2 by a factor of about 3. For MgMOF-74, NaX, and CuBTTri, the use of IAST predicts a significant decrease in S_{ads} with increasing total pressure, p_t; see Figure 1a. The decrease in S_{ads} with increasing p_t is due to entropy effects that favor H_2 owing to its higher $q_{i,sat}$ value. For MgMOF-74, the decrease in S_{ads} is from 1500 at 0.2 MPa to a value of 500 at 6 MPa. The more attractive a MOF is, the greater is the need for accurate calculation of adsorption equilibria using IAST; the mixed-gas Langmuir model will be overly optimistic with regard to separation selectivities. By the same token, for MOFs such as MOF-177 and BeBTB, that have low promise with regard to CO_2/H_2 separations, S_{ads} is seen to be practically independent of p_t; it is sufficient to use the mixed-gas Langmuir model. The separation performance of Co(BDP) is an oddity in that S_{ads} *increases* with p_t. This increase can be traced to the steep rise in the CO_2 loadings, caused by structural changes,[33,34] when the partial pressure rises above 0.2 MPa; see pure component isotherm data in Figure 3.

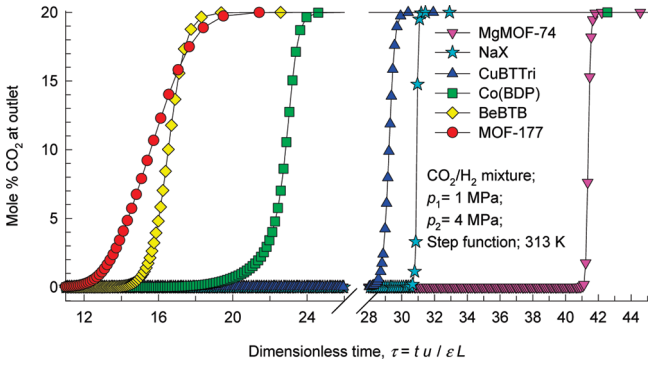

Figure 4. Breakthrough curves showing the mole % CO_2 in the outlet of packed bed adsorber with step-input of 20/80 CO_2/H_2 mixture at a total pressure of 5 MPa and 313 K.

It should be noted that the applicability of the IAST is restricted to cases in which there is a homogeneous distribution of adsorbate species throughout the microporous framework. The IAST predictions will fail when segregation effects are present. Examples of segregated adsorption include preferential siting of CO_2 at the window regions,[51,56,57] or preferential location at the intersections of network of channels.[58]

Also it is to be noted that, although we have done so, it is not clear that IAST can be applied to flexible MOFs such as Co(BDP), because of the potential for one component of a gas mixture to trigger pore opening[59] and thereby facilitate the adsorption of another component. Coudert et al.[60−62] have developed modifications to the IAST to account for structural changes, but their theory needs experimental validation, and some validation experiments are beginning to appear in the published literature.[63]

The need for rigorous use of the IAST in PSA modeling has been stressed in several papers.[48,64,65] For separation of alkane isomers in PSA units with MFI zeolite, the use of IAST is of vital importance because the obtained selectivities result from differences in saturation capacities and entropy effects.[48,64,66] Jeon et al.[65] modeled a PSA unit for CO_2/N_2 separation using NaX zeolite and found that the predictions using IAST were in good agreement with experimental data. In contrast, the mixed-gas Langmuir model gave extremely poor predictions of PSA performance.

The set of partial differential equations (PDEs) (2) and (4) are first subjected to finite volume discretization. Typically, the adsorber length L is divided into 100 or more slices. Each crystallite, assumed to be spherical, is divided into 10−20 equivolume slices. The number of slices is determined by checking that the obtained breakthrough results do not change on increasing it. Combination of the discretized PDEs along with the algebraic IAST equilibrium model results in a set of differential-algebraic equations (DAEs), which are solved using BESIRK.[67] BESIRK is a sparse matrix solver, based on the semi-implicit Runge−Kutta method originally developed by Michelsen[68] and extended with the Bulirsch−Stoer extrapolation method.[69] Use of BESIRK improves the numerical solution efficiency in solving the set of DAEs. The evaluation of the sparse Jacobian required in the numerical algorithm is largely based on analytic expressions.[48] Further details of the adsorber model, along with the numerical procedures used in this work, are provided by Krishna and co-workers.[48,70,71] Typical computation times for a binary gas mixture breakthrough

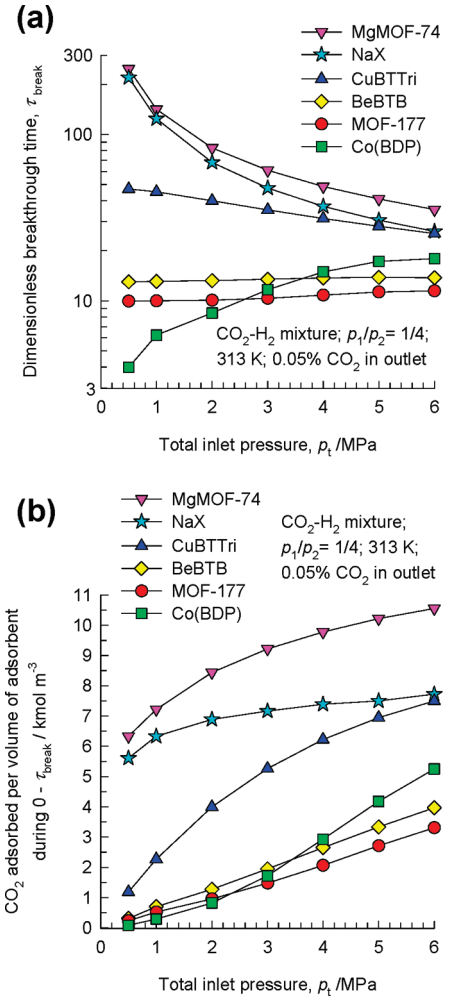

Figure 5. Dependence of (a) dimensionless breakthrough time, τ_{break} and (b) number of moles of CO_2 adsorbed per m^3 of adsorbent material during the time interval 0−τ_{break}, on the inlet pressure, p_t, of a packed bed adsorber with step-input of a 20/80 CO_2/H_2 mixture operating at 313 K.

are less than 200 s, allowing such transient adsorber calculations to be routinely used for screening purposes.

Since the primary objective of this communication is the ranking of MOFs, rather than detailed process design, we proceed further assuming that there are no intracrystalline diffusion limitations, and thermodynamic equilibrium prevails everywhere within the bed. With these assumptions, eq 3 simplifies to give

$$\overline{q}_i = q_i \tag{8}$$

The assumption of thermodynamic equilibrium is a good one when the crystallite sizes are sufficiently small and the intracrystalline diffusivities are sufficiently large. Most of the MOFs that we shall consider in this paper have characteristic pore dimensions of the order of 1 nm or larger. In these cases, the assumption of negligible intracrystalline diffusion resistance is a reasonably good one to make in practice.

3. TRANSIENT BREAKTHROUGH CALCULATIONS

Figure 4 presents typical data for the mole % CO_2 in the outlet gas mixture exiting from a packed bed adsorber subjected to a step-input of a 20/80 CO_2/H_2 mixture at inlet pressure of

dx.doi.org/10.1021/jp202203c |J. Phys. Chem. C 2011, 115, 12941–12950

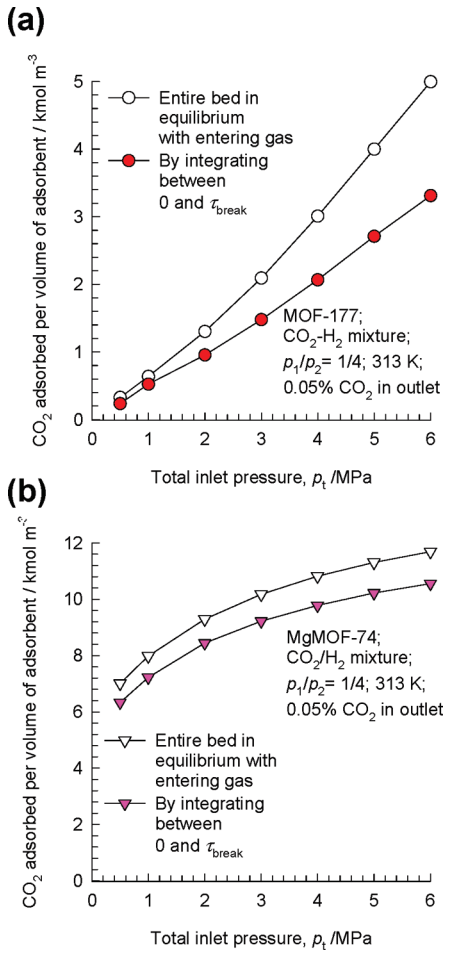

Figure 6. Comparison of the calculations of moles of CO_2 adsorbed per m^3 of adsorbent material in (a) MOF-177 and (b) MgMOF-74 using two different approaches: (1) by integrating the loadings during the time interval $0-\tau_{break}$ and (2) assuming that the entire bed is in equilibrium with the incoming gas mixture.

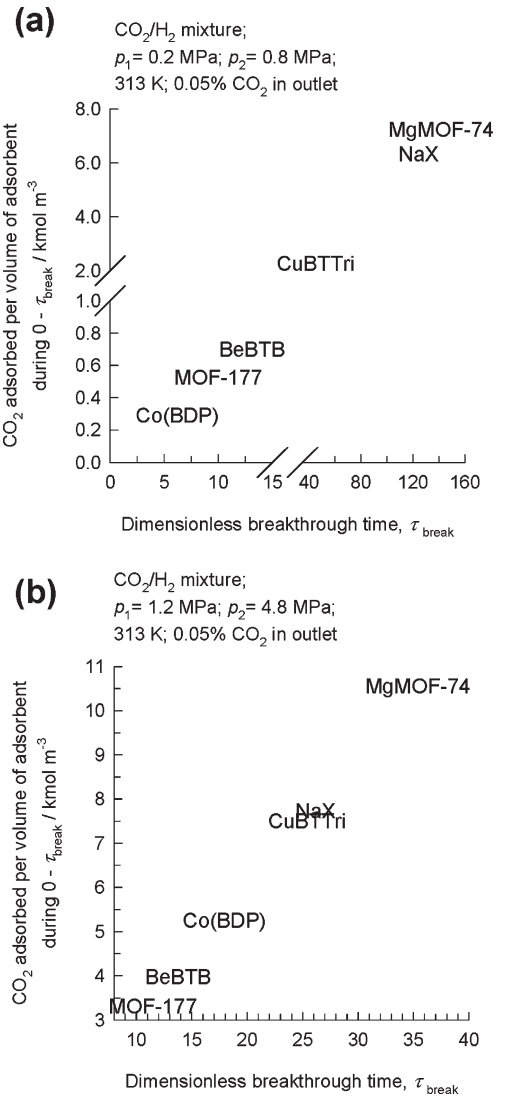

Figure 7. Plots of the number of moles of CO_2 adsorbed per m^3 of adsorbent material during the time interval $0-\tau_{break}$ against the breakthrough time τ_{break} for packed bed adsorber with step-input of a 20/80 CO_2/H_2 mixture at 313 K and total pressures of (a) 1 MPa and (b) 6 MPa. The breakthrough times, τ_{break}, correspond to those when the outlet gas contains 0.05 mol % CO_2.

p_t = 5 MPa. These breakthrough calculations were performed for an adsorber of fixed volume and the same voidage fraction, ε. Consequently, the mass of adsorbent material used is different and determined by the values of the framework densities of BeBTB, MOF-177, Co(BDP), CuBTTri, MgMOF-74, and NaX which are, 423, 426, 721, 773, 905, and 1421 kg m^{-3}, respectively. The x axis is a *dimensionless* time, τ, obtained by dividing the actual time, t, by the contact time between the gas and the crystallites, $\varepsilon L/u$. For a given adsorbent, under chosen operating conditions, the breakthrough characteristics are uniquely defined by τ, allowing the results to be presented here to be equally applicable to laboratory scale equipment as well as to industrial scale adsorbers.

Materials that have high values of S_{ads}: MgMOF-74, NaX, and CuBTTri, exhibit steep, near-vertical, breakthrough characteristics. For Co(BDP), BeBTB, and MOF-177, which have relatively low values of S_{ads}, the increase in the mole % CO_2 in the outlet gas occurs in a more gradual manner.

For H_2 production with a specified level of purity, assumed here to be 0.05 mol % CO_2, the breakthrough times, τ_{break}, can be determined. Figure 5a shows the dependence of τ_{break} on the inlet pressure, p_t. A cursory examination indicates that the hierarchy of τ_{break} values for different structures follows the S_{ads} vs p_t data trends in Figure 1a. However, there are some τ_{break} vs p_t characteristics that require further examination and elucidation. For example, the τ_{break} of CuBTTri gets progressively closer to that of NaX with increasing p_t, and at 6 MPa, the breakthrough times are nearly the same. This is remarkable, in view of the fact that the S_{ads} of CuBTTri is significantly lower than that of NaX for the *entire range* of p_t; see Figure 1a. The explanation lies in the significant increase in the working capacity of CuBTTri when p_t is increased beyond 1 MPa; see Figure 1b. This increase in Δq has the effect of delaying the breakthrough of CO_2. In contrast, the working capacity of NaX reaches a plateau value and ceases to increase beyond 1 MPa. For this reason, the decrease in τ_{break} with increasing p_t is more pronounced for NaX than that for CuBTTri. Similarly, we find that the τ_{break} for Co(BDP) is significantly higher than for MOF-177 and BeBTB at 6 MPa, which can be explained by the stronger increase in Δq with

dx.doi.org/10.1021/jp202203c |J. Phys. Chem. C 2011, 115, 12941–12950

increased pressure; cf. Figure 1b. Such capacity advantages become more telling at higher pressures. Thus, the breakthrough times, which reflect a combination of selectivity and capacity considerations, are a more appropriate yardstick for comparing MOFs with regard to performance in PSA units.

When the desired level of purity is attained, the adsorption step is terminated at $\tau = \tau_{break}$, and the bed has to be regenerated. The amount of CO_2 captured during the time interval $0-\tau_{break}$, expressed in terms of the number of moles of CO_2 adsorbed within the bed per m^3 of adsorbent material, can be determined from a mass balance on the adsorber, as plotted in Figure 5b. Here, there are some important differences with the working capacity data of Figure 1b. The consequence of the gradual increase in mole % CO_2 in the exit gas for MOFs such as BeBTB, MOF-177, and Co(BDP), made evident in Figures 4, is that the contents of the bed are removed from steady state when operation is stopped at $\tau = \tau_{break}$. To illustrate this, Figure 6a presents a comparison of two sets of calculations of the amount of CO_2 adsorbed in a PSA unit containing MOF-177 (1) by integrating the loadings during the time interval $0-\tau_{break}$ from the breakthrough calculations and (2) assuming that the entire bed is in equilibrium with the incoming gas mixture. Importantly, the assumption of the entire bed being in equilibrium results in an overestimation of the amount of CO_2 adsorbed by up to 50%. Similar conclusions hold for Co(BDP) and BeBTB. Thus, low adsorption selectivity also results in underutilization of the adsorber bed. In contrast, for MgMOF-74, NaX, and CuBTTri, the entire bed is nearly at steady state at $\tau = \tau_{break}$, and the two sets of calculations are only marginally different as illustrated in Figure 6b for MgMOF-74. Higher adsorption selectivities therefore also result in better bed utilization.

For screening purposes, it is useful to make plots of the amount of CO_2 adsorbed during the time interval $0-\tau_{break}$, against τ_{break}; see Figure 7. A longer τ_{break} is desirable because the frequency of regeneration is reduced. MgMOF-74 occupies the desirable top right-hand corner and can therefore be regarded as best adsorbent, from the standpoint of both productivity and frequency of regeneration. It is also interesting to note that for 1 MPa operation, Figure 7a will lead us to conclude that the separation performance of NaX is significantly superior to that of CuBTTri. However, for 6 MPa operation, CuBTTri is able to adsorb nearly as much CO_2 as NaX, and this is largely attributable to a significant increase in the working capacity of CuBTTri at increased pressures. The data in Figure 7 clearly indicate the shortcomings of traditionally used zeolite NaX which is typically used in high-pressure PSA units for H_2 purification, compared to certain MOFs with exposed metal cation sites, and MgMOF-74 in particular.

For MOF-177, BeBTB, and Co(BDP) the high working capacities cannot compensate for the extremely low S_{ads} values; therefore all of these structures end up in the undesirable bottom-left corner of the two plots in Figure 7.

For separation of CO_2/CH_4 mixtures, Bao et al.[72] have conducted experiments to compare the selectivity and capacity of MgMOF-74 with NaX, in the pressure range of 0−0.1 MPa. Their data show similar values of S_{ads} for both materials, but a significantly higher capacity for MgMOF-74. On the basis of this evidence we should expect superior PSA performance with MgMOF-74, especially at higher pressures. To seek confirmation of this expectation, we determined adsorber breakthroughs for the range of pressures 0.5−5 MPa. Typical breakthrough curves, for $p_t = 5$ MPa are shown in Figure 8a. We note the steep, near-vertical, breakthrough curves that are characteristic of materials with high S_{ads}. As plotted in Figure 8b, a comparison of

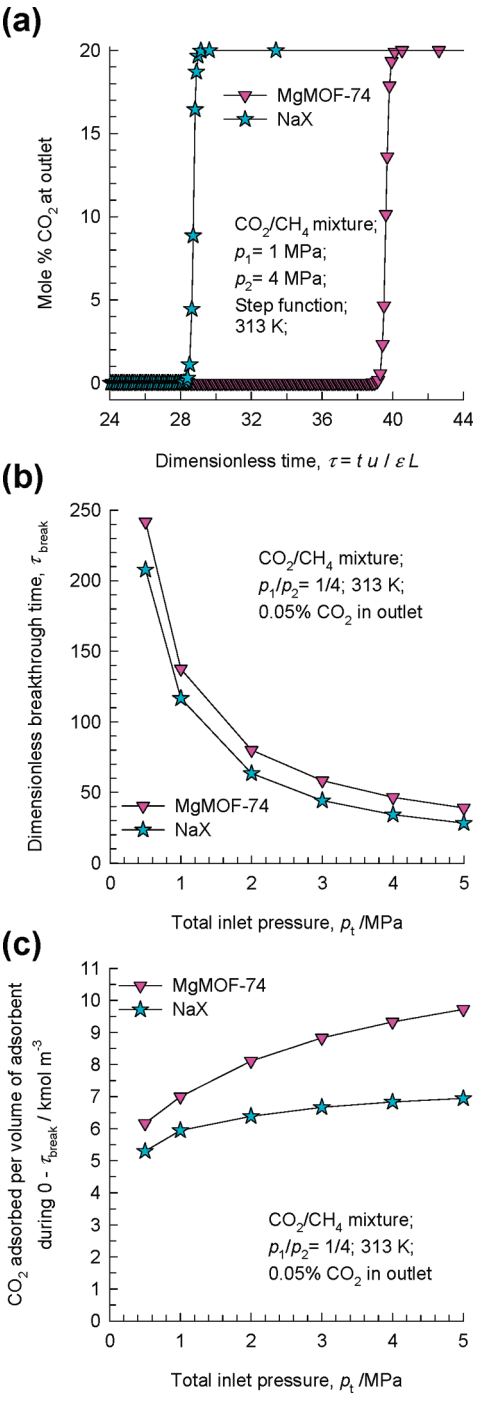

Figure 8. (a) Mole % CO_2 in the outlet of adsorber, packed with MgMOF-74 or NaX, with step-input of a 20/80 CO_2/CH_4 mixture at a total pressure 5 MPa and 313 K. (b, c) Dependence of (b) dimensionless breakthrough time, τ_{break}, and (c) moles of CO_2 adsorbed per m^3 of adsorbent material during the time interval $0-\tau_{break}$, on the inlet pressure, p_t. The dual-site Langmuir−Freundlich fits of the pure component isotherms of CO_2 and H_2 adsorption isotherms are based on the experimental data of Herm et al.,[37] Dietzel et al.,[30] Belmabkhout et al.,[76] and Cavenati et al.[77] The Supporting Information accompanying this publication contains the dual Langmuir−Freundlich fit constants.

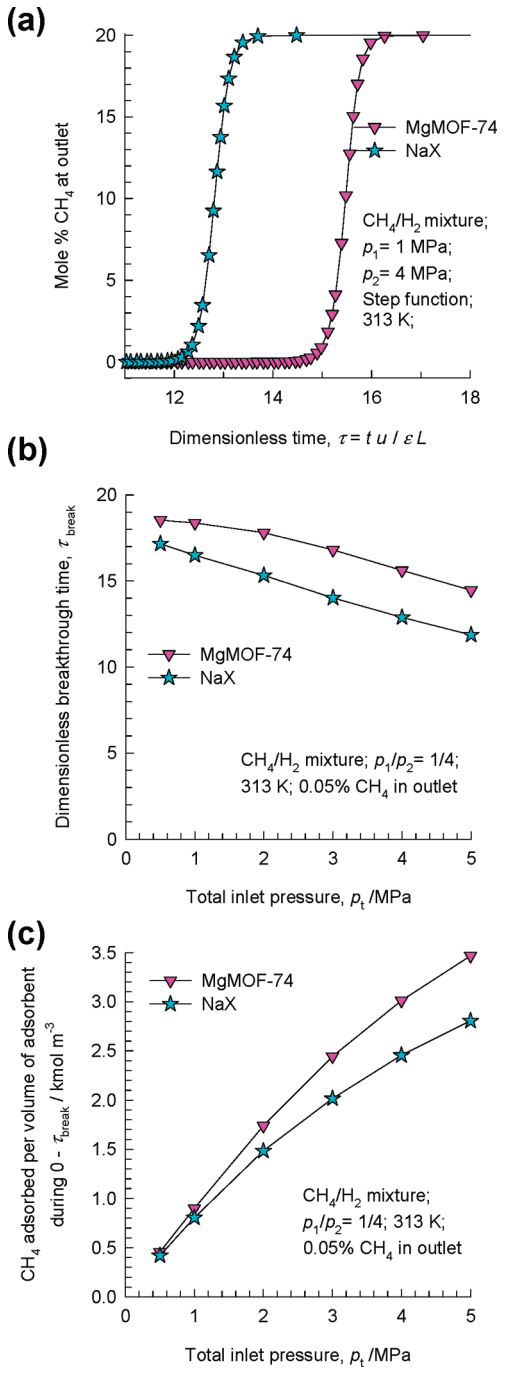

Figure 9. (a) Mole % CH_4 in the outlet of an adsorber, packed with MgMOF-74 or NaX, with step-input of a 20/80 CH_4/H_2 mixture at a total pressure of 5 MPa and 313 K. (b, c) Dependence of (b) dimensionless breakthrough time, τ_{break}, and (c) moles of CH_4 adsorbed per m^3 of adsorbent material during the time interval $0-\tau_{break}$, on the inlet pressure, p_t. The dual-site Langmuir−Freundlich fits of the pure component isotherms of CO_2 and H_2 adsorption isotherms are based on the experimental data of Herm et al.,[37] Dietzel et al.,[30] Belmabkhout et al.,[76] and Cavenati et al.[77] The Supporting Information accompanying this publication contains the dual Langmuir−Freundlich fit constants.

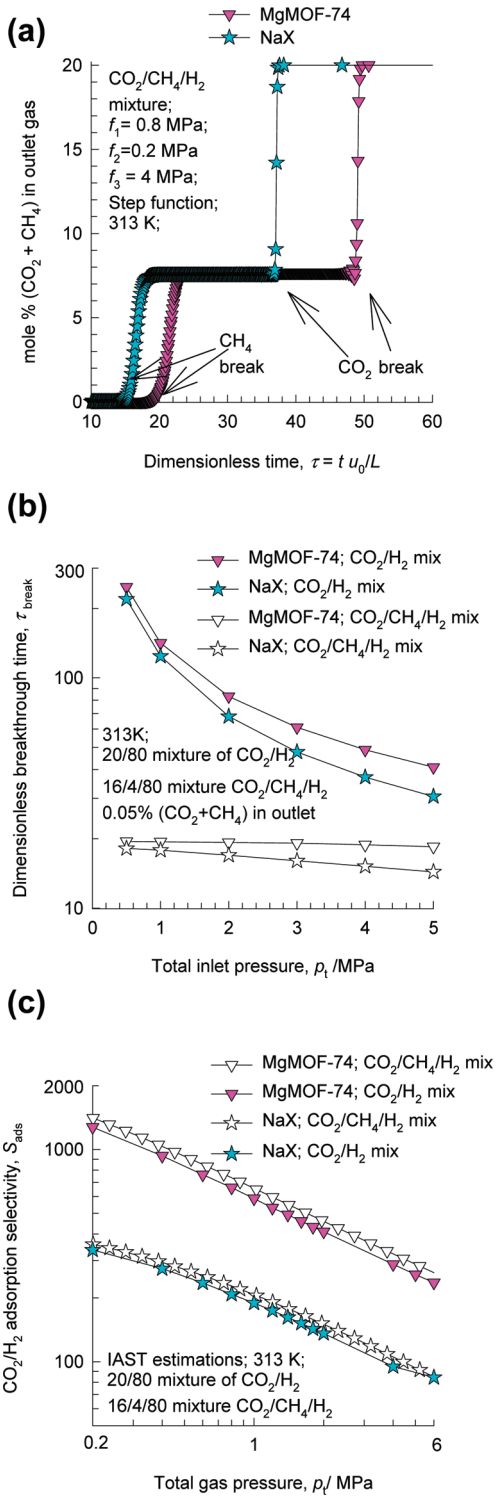

Figure 10. (a) Mole % (CH_4 + CO_2) in the outlet of an adsorber, packed with MgMOF-74 and NaX, with step-input of a 4/16/80 $CH_4/CO_2/H_2$ gas mixture at a total pressure of 5 MPa and 313 K. Video animations of the breakthrough dynamics are available as Supporting Information. (b) Dependence of dimensionless breakthrough times, τ_{break}, on the inlet pressure, p_t. The calculations are presented for MgMOF-74 and zeolite NaX for both 20/80 CO_2/H_2 and 4/16/80 $CH_4/CO_2/H_2$ mixtures. (c) IAST calculations of the CO_2/H_2 adsorption selectivities for 20/80 CO_2/H_2 and 4/16/80 $CH_4/CO_2/H_2$ mixtures.

the breakthrough times shows that MgMOF-74 performs consistently better than NaX. The more important advantage of MgMOF-74 over NaX, however, is that a significantly higher amount of CO_2

can be adsorbed; see Figure 8c. Indeed, at inlet pressures above 0.5 MPa, a PSA unit filled with MgMOF-74 can be expected to exhibit about 50% higher CO_2 capacity compared to one containing zeolite NaX.

For H_2 production from steam reforming of natural gas, the separation of CH_4/H_2 mixtures is required.[73,74] Due to the significantly lower adsorption strength of CH_4, compared to CO_2, the breakthrough curves for both MgMOF-74 and zeolite NaX show a gradual approach to steady-state; see Figure 9a. The breakthrough times for a range of pressures are shown in Figure 9b. It is noteworthy that these breakthrough times are significantly shorter for both the materials than observed earlier for CO_2/H_2 and CO_2/CH_4 mixtures; this is a consequence of the significantly lower S_{ads} for a CH_4/H_2 separation. The data for the amount of CH_4 adsorbed during the time interval $0-\tau_{break}$ are presented in Figure 9c. Here again, MgMOF-74 emerges as the more attractive material when compared to the traditional NaX zeolite, from the points of view of both reduced frequency of regeneration and productivity. Given the more gradual breakthrough characteristics apparent in Figure 9a, the amount of CH_4 adsorbed is lower than that calculated assuming that the entire bed is in equilibrium with the incoming gas mixture.

For H_2 purification processes from gaseous streams containing both CH_4 and CO_2, the breakthrough characteristics are primarily dictated by the more poorly adsorbing impurity, CH_4. To illustrate this Figure 10a shows the total mol % "impurity" exiting from an adsorber fed with a 4/16/80 $CH_4/CO_2/H_2$ gas mixture at a total pressure of 5 MPa and 313 K. CH_4 breaks through significantly earlier than CO_2 for both zeolite NaX and MgMOF-74. The breakthrough times for NaX are lower than those for MgMOF-74; see Figure 10b. We also note that the breakthrough times for the ternary $CH_4/CO_2/H_2$ mixture are significantly lower, by a factor of about 5, than those for the corresponding binary 20/80 CO_2/H_2 mixture. This demonstrates the strong influence of a small amount (4%) of CH_4 on PSA performance, and underscores the need for careful analysis of *all* impurities in a gas mixture and not just the predominant one. In sharp contrast to the strong influence on τ_{break}, the adsorption selectivity S_{ads} for CO_2/H_2 separation is hardly influenced by the presence of 4% CH_4; see Figure 10c. We conclude that the metric τ_{break} is a much more sensitive measure of the influence of trace components in the feed to a PSA unit.

4. CONCLUSIONS

With published experimental data on pure component isotherms for CO_2, CH_4, and H_2 at 313 K in five different MOFs, along with zeolite NaX, the dynamics of breakthrough of CO_2/H_2, CO_2/CH_4, CH_4/H_2, and $CO_2/CH_4/H_2$, mixtures in a packed bed adsorber were calculated for a range of pressures. The following major conclusions emerge from this study.

(1) The dimensionless breakthrough time, τ_{break}, is influenced not only by the adsorption selectivity, S_{ads}, but also by the working capacity, Δq. A high value of τ_{break} is desirable in practice because it reduces the frequency of required regeneration.

(2) The amount of component adsorbed during the interval $0-\tau_{break}$ is a measure of the productivity of the PSA unit.

(3) Materials with high S_{ads} have near-vertical breakthrough characteristics and τ_{break} is only slightly lower than the time required for the bed to reach steady state. In this case, the amount of gas adsorbed during the interval $0-\tau_{break}$ can be estimated using the assumption that the entire bed is in equilibrium with the incoming gas mixture. When S_{ads} is low, portions of the bed are not fully utilized, since they are not in equilibrium with the entering gas mixture.

(4) For separation of CO_2/H_2, CO_2/CH_4, and CH_4/H_2 mixtures, MgMOF-74 emerges as the best material, from the viewpoints of both frequency of regeneration and productivity. The advantage of MgMOF-74 over traditionally used NaX zeolite is particularly evident at pressures exceeding 1 MPa.

(5) For screening of MOFs and zeolites, the suggested metric τ_{break} provides the proper degree of discrimination between the variety of factors that govern PSA separations. It, together with the amount of gas adsorbed during the interval $0-\tau_{break}$, should be considered the most useful single metric for ranking adsorbents. Diagrams such as those presented in Figure 7 are very useful in deciding on the choice of the ideal MOF.

The screening strategy suggested in this paper can be considered as the initial one based only on information on pure component isotherms and assumption of thermodynamic equilibrium. The next step would be to consider the influence of intracrystalline diffusion and include the solution of eq 4 in the breakthrough calculations. Inclusion of intracrystalline diffusion would have the effect of broadening the breakthrough curves. Such broadening will lead to a reduction in the amount that is effectively adsorbed. Other practical issues such as thermal stability, influence of the presence of small quantities of water,[75] and ease of regeneration also need to be taken into consideration at subsequent stages in the process of selection of the ideal adsorbent material for a given separation task.

■ ASSOCIATED CONTENT

Supporting Information. This material includes a document containing the dual Langmuir−Freundlich fit constants for pure component isotherms for CO_2, CH_4, and H_2 in the variety of MOFs and NaX, comparisons of the fits with the experimental data, validations of the IAST by using Configurational-Bias Monte Carlo simulations of CO_2/H_2 mixture adsorption, and video animations of the breakthrough dynamics of $CO_2/CH_4/H_2$ in adsorbers packed with MgMOF-74 and NaX. This material is available free of charge via the Internet at http://pubs.acs.org.

■ AUTHOR INFORMATION

Corresponding Author
*E-mail: r.krishna@uva.nl.

■ ACKNOWLEDGMENT

This material is based upon work supported as part of the Center for Gas Separations Relevant to Clean Energy Technologies, an Energy Frontier Research Center funded by the U.S. Department of Energy, Office of Science, Office of Basic Energy Sciences under Award Number DE-SC0001015.

■ NOTATION

b_i	dual Langmuir−Freundlich constant for species i, $Pa^{-\nu_i}$
L	length of packed bed adsorber, m
n	number of components in mixture, dimensionless

N_i	molar flux of species i for intraparticle radial diffusion, mol m^{-2} s^{-1}
p_i	partial pressure of species i in mixture, Pa
p_t	total system pressure, Pa
q_i	component molar loading of species i, mol kg^{-1}
$q_{i,sat}$	saturation loading of species i, mol kg^{-1}
Δq	working capacity, mol kg^{-1}
r	radial distance coordinate, m
r_c	radius of crystallite, m
R	gas constant, 8.314 J mol^{-1} K^{-1}
S_{ads}	adsorption selectivity, dimensionless
t	time, s
T	temperature, K
T_c	critical temperature, K
u	superficial gas velocity entering the packed bed, m s^{-1}
V_p	accessible pore volume, m^3 kg^{-1}
z	distance along the adsorber, m

Greek Letters

ε	voidage of packed bed, dimensionless
ν_i	exponent in the dual Langmuir−Freundlich isotherm, dimensionless
ρ	framework density, kg m^{-3}
τ	time, dimensionless
τ_{break}	breakthrough time, dimensionless

Subscripts

i	referring to component i
t	referring to total mixture

REFERENCES

(1) Murray, L. J.; Dincă, M.; Long, J. R. *Chem. Soc. Rev.* **2009**, *38*, 1294–1314.
(2) Xiang, S.; Zhou, W.; Gallegos, J. M.; Liu, Y.; Chen, B. *J. Am. Chem. Soc.* **2009**, *131*, 12415–12419.
(3) Furukawa, H.; Ko, N.; Go, Y. B.; Aratani, N.; Choi, S. B.; Choi, E.; Yazaydin, A. O.; Snurr, R. Q.; O'Keeffe, M.; Kim, J.; Yaghi, O. M. *Science* **2010**, *329*, 424–428.
(4) Li, J. R.; Kuppler, R. J.; Zhou, H. C. *Chem. Soc. Rev.* **2009**, *38*, 1477–1504.
(5) Keskin, S.; van Heest, T. M.; Sholl, D. S. *ChemSusChem* **2010**, *3*, 879–891.
(6) D'Alessandro, D. M.; Smit, B.; Long, J. R. *Angew. Chem., Int. Ed.* **2010**, *49*, 6058–6082.
(7) Férey, G.; Serre, C.; Devic, T.; Maurin, G.; Jobic, H.; Llewellyn, P. L.; De Weireld, G.; Vimont, A.; Daturi, M.; Chang, J. S. *Chem. Soc. Rev.* **2011**, *40*, 550–562.
(8) Krishna, R.; van Baten, J. M. *J. Membr. Sci.* **2010**, *360*, 323–333.
(9) Krishna, R.; van Baten, J. M. *Phys. Chem. Chem. Phys.* **2011**, *13*, 10593–10616.
(10) Zhao, D.; Timmons, D. J.; Yuan, D.; Zhou, H. *Acc. Chem. Res.* **2011**, *44*, 123–133.
(11) An, J.; Rosi, N. L. *J. Am. Chem. Soc.* **2010**, *132*, 5578–5579.
(12) Babarao, R.; Jiang, J. *J. Am. Chem. Soc.* **2009**, *131*, 11417–11425.
(13) Britt, D.; Furukawa, H.; Wang, B.; Glover, T. G.; Yaghi, O. M. *Proc. Natl. Acad. Sci. U.S.A.* **2009**, *106*, 20637–20640.
(14) Caskey, S. R.; Wong-Foy, A. G.; Matzger, A. J. *J. Am. Chem. Soc.* **2008**, *130*, 10870–10871.
(15) Yazaydın, A. Ö.; Benin, A. I.; Faheem, S. A.; Jakubczak, P.; Low, J. J.; Willis, R. R.; Snurr, R. Q. *Chem. Mater.* **2009**, *21*, 1425–1430.
(16) Yazaydın, A. Ö.; Snurr, R. Q.; Park, T. H.; Koh, K.; Liu, J.; LeVan, M. D.; Benin, A. I.; Jakubczak, P.; Lanuza, M.; Galloway, D. B.; Low, J. J.; Willis, R. R. *J. Am. Chem. Soc.* **2009**, *131*, 18198–18199.
(17) Bae, Y. S.; Farha, O. K.; Hupp, J. T.; Snurr, R. Q. *J. Mater. Chem.* **2009**, *19*, 2131–2134.
(18) Arstad, B.; Fjellvåg, H.; Kongshaug, K. O.; Swang, O.; Blom, R. *Adsorption* **2008**, *14*, 755–762.
(19) Vaidhyanathan, R.; Iremonger, S. S.; Dawson, K. W.; Shimizu, G. K. H. *Chem. Commun.* **2009**, 5230–5232.
(20) Torrisi, A.; Mellot-Draznieks, C.; Bell, R. G. *J. Chem. Phys.* **2009**, *130*, 194703.
(21) An, J.; Geib, S. J.; Rosi, N. L. *J. Am. Chem. Soc.* **2010**, *132*, 38–39.
(22) Torrisi, A.; Bell, R. G.; Mellot-Draznieks, C. *Cryst. Growth Des.* **2010**, *10*, 2839–2841.
(23) Demessence, A.; D'Alessandro, D. M.; Foo, M. W.; Long, J. R. *J. Am. Chem. Soc.* **2009**, *131*, 8784–8786.
(24) Couck, S.; Denayer, J. F. M.; Baron, G. V.; Rémy, T.; Gascon, J.; Kapteijn, F. *J. Am. Chem. Soc.* **2009**, *131*, 6326–6327.
(25) Deng, H.; Doonan, C. J.; Furukawa, H.; Ferreira, R. B.; John Towne, J.; Knobler, C. B.; Wang, B.; Yaghi, O. M. *Science* **2010**, *327*, 846–850.
(26) Karra, J. R.; Walton, K. S. *J. Phys. Chem. C* **2010**, *114*, 15735–15740.
(27) Myers, A. L.; Prausnitz, J. M. *AIChE J.* **1965**, *11*, 121–130.
(28) Rosi, N. L.; Kim, J.; Eddaoudi, M.; Chen, B.; O'Keeffe, M.; Yaghi, O. M. *J. Am. Chem. Soc.* **2005**, *127*, 1504–1518.
(29) Dietzel, P. D. C.; Panella, B.; Hirscher, M.; Blom, R.; Fjellvåg, H. *Chem. Commun.* **2006**, 959–961.
(30) Dietzel, P. D. C.; Besikiotis, V.; Blom, R. *J. Mater. Chem.* **2009**, *19*, 7362–7370.
(31) Chae, H. K.; Siberio-Pérez, D. Y.; Kim, J.; Go, Y. B.; Eddaoudi, M.; Matzger, A. J.; O'Keeffe, M.; Yaghi, O. M. *Nature* **2004**, *427*, 523–527.
(32) Sumida, K.; Hill, M. R.; Horike, S.; Dailly, A.; Long, J. R. *J. Am. Chem. Soc.* **2009**, *131*, 15120–15121.
(33) Choi, H. J.; Dincă, M.; Long, J. R. *J. Am. Chem. Soc.* **2008**, *130*, 7848–7850.
(34) Salles, F.; Maurin, G.; Serre, C.; Llewellyn, P. L.; Knöfel, C.; Choi, H. J.; Filinchuk, Y.; Oliviero, L.; Vimont, A.; Long, J. R.; Férey, G. *J. Am. Chem. Soc.* **2010**, *132*, 13782–13788.
(35) Ho, M. T.; Allinson, G. W.; Wiley, D. E. *Ind. Eng. Chem. Res.* **2008**, *47*, 4883–4890.
(36) Hamon, L.; Jolimaitre, E.; Pirngruber, G. *Ind. Eng. Chem. Res.* **2010**, *49*, 7497–7503.
(37) Herm, Z. R.; Swisher, J. A.; Smit, B.; Krishna, R.; Long, J. R. *J. Am. Chem. Soc.* **2011**, *133*, 5664–5667.
(38) Kumar, R. *Ind. Eng. Chem. Res.* **1994**, *33*, 1600–1605.
(39) Bastin, L.; Bárcia, P. S.; Hurtado, E. J.; Silva, J. A. C.; Rodrigues, A. E.; Chen, B. *J. Phys. Chem. C* **2008**, *112*, 1575–1581.
(40) Jadhav, P. D.; Rayalu, S. S.; Biniwale, R. B.; Devotta, S. *Curr. Sci.* **2007**, *92*, 724–726.
(41) Britt, D.; Tranchemontagne, D.; Yaghi, O. M. *Proc. Natl. Acad. Sci. U.S.A.* **2008**, *105*, 11623–11627.
(42) Ruthven, D. M. *Principles of Adsorption and Adsorption Processes*; John Wiley: New York, 1984.
(43) Ruthven, D. M.; Farooq, S.; Knaebel, K. S. *Pressure swing adsorption*; VCH Publishers: New York, 1994.
(44) Yang, R. T. *Gas separation by adsorption processes*; Butterworth: Boston, 1987.
(45) Do, D. D. *Adsorption analysis: Equilibria and kinetics*; Imperial College Press: London, 1998.
(46) van den Broeke, L. J. P.; Krishna, R. *Chem. Eng. Sci.* **1995**, *50*, 2507–2522.
(47) Walton, K. S.; LeVan, M. D. *Ind. Eng. Chem. Res.* **2003**, *42*, 6938–6948.
(48) Krishna, R.; Baur, R. *Sep. Purif. Technol.* **2003**, *33*, 213–254.
(49) Krishna, R. *J. Phys. Chem. C* **2009**, *113*, 19756–19781.
(50) Krishna, R.; van Baten, J. M. *Microporous Mesoporous Mater.* **2008**, *109*, 91–108.
(51) Krishna, R.; van Baten, J. M. *Chem. Eng. Sci.* **2008**, *63*, 3120–3140.
(52) Walton, K. S.; Millward, A. R.; Dubbeldam, D.; Frost, H.; Low, J. J.; Yaghi, O. M.; Snurr, R. Q. *J. Am. Chem. Soc.* **2008**, *130*, 406–407.

(53) Krishna, R.; van Baten, J. M. *Langmuir* **2010**, *26*, 3981–3992.
(54) Krishna, R.; van Baten, J. M. *Langmuir* **2010**, *26*, 8450–8463.
(55) Rao, M. B.; Sircar, S. *Langmuir* **1999**, *15*, 7258–7267.
(56) Krishna, R.; van Baten, J. M. *Chem. Phys. Lett.* **2007**, *446*, 344–349.
(57) Krishna, R.; van Baten, J. M. *Sep. Purif. Technol.* **2008**, *61*, 414–423.
(58) Krishna, R.; van Baten, J. M. *Chem. Eng. J.* **2008**, *140*, 614–620.
(59) Dubbeldam, D.; Krishna, R.; Snurr, R. Q. *J. Phys. Chem. C* **2009**, *113*, 19317–19327.
(60) Coudert, F. X.; Jeffroy, M.; Fuchs, A. H.; Boutin, A.; Mellot-Draznieks, C. *J. Am. Chem. Soc.* **2008**, *130*, 14294–14302.
(61) Coudert, F. X.; Mellot-Draznieks, C.; Fuchs, A. H.; Boutin, A. *J. Am. Chem. Soc.* **2009**, *131*, 3442–3443.
(62) Coudert, F. X.; Mellot-Draznieks, C.; Fuchs, A. H.; Boutin, A. *J. Am. Chem. Soc.* **2009**, *131*, 11329–11331.
(63) Boutin, A.; Couck, S.; Coudert, F. X.; Serra-Crespo, P.; Gascon, J.; Kapteijn, F.; Fuchs, A. H.; Denayer, J. F. M. *Microporous Mesoporous Mater.* **2011**, *140*, 108–113.
(64) Krishna, R.; Baur, R. *Chem. Eng. Sci.* **2005**, *60*, 1155–1166.
(65) Jeon, J. K.; Ihm, S. K.; Park, Y. K.; Kim, J. S.; Kim, S. D.; Kim, S.; Kim, J. M.; Kim, S. S.; Yoo, K. S. *Stud. Surf. Sci. Catal.* **2004**, *153*, 547–550.
(66) Krishna, R.; Smit, B.; Calero, S. *Chem. Soc. Rev.* **2002**, *31*, 185–194.
(67) Kooijman, H. A.; Taylor, R. *AIChE J.* **1995**, *41*, 1852–1863.
(68) Michelsen, M. *AIChE J.* **1976**, *22*, 594–597.
(69) Bulirsch, R.; Stoer, J. *Numer. Math.* **1966**, *8*, 1–14.
(70) Krishna, R.; Baur, R. *Diffusion, Adsorption and Reaction in Zeolites: Modelling and Numerical Issues*; University of Amsterdam, 11 November 2003, http://www.science.uva.nl/research/cr/zeolite/.
(71) Krishna, R.; van Baten, J. M. *J. Membr. Sci.* **2011**, http://dx.doi.org/10.1016/j.memsci.2011.05.001.
(72) Bao, Z.; Yu, L.; Ren, Q.; Lu, X.; Deng, S. *J. Colloid Interface Sci.* **2011**, *353*, 549–556.
(73) Gallo, M.; Glossman-Mitnik, D. *J. Phys. Chem. C* **2009**, *113*, 6634–6642.
(74) Keskin, S. *Ind. Eng. Chem. Res.* **2010**, *49*, 11689–11696.
(75) Kizzie, A. C.; Wong-Foy, A. G.; Matzger, A. J. *Langmuir* **2011**, *27*, 6368–6373.
(76) Belmabkhout, Y.; Pirngruber, G.; Jolimaitre, E.; Methivier, A. *Adsorption* **2007**, *13*, 341–349.
(77) Cavenati, S.; Grande, C. A.; Rodrigues, A. E. *J. Chem. Eng. Data* **2004**, *49*, 1095–1101.